Synthesis of Optimal 5G Array Layouts With Wide-Angle Scanning and Zooming Ability for Efficient Link Setup and High-QoS Communication

Aslan, Yanki; Roederer, Antoine; Yarovoy, Alexander

DOI
10.1109/LAWP.2020.3006314

Publication date
2020

Document Version
Final published version

Published in
IEEE Antennas and Wireless Propagation Letters

Synthesis of Optimal 5G Array Layouts With Wide-Angle Scanning and Zooming Ability for Efficient Link Setup and High-QoS Communication

Yanki Aslan, *Graduate Student Member, IEEE*, Antoine Roederer, *Life Fellow, IEEE*, and Alexander Yarovoy, *Fellow, IEEE*

***Abstract*—An irregular antenna synthesis technique with jointly optimized array subset layouts has been proposed for efficient beam setup and reliable communication in 5G. The proposed approach addresses both the electromagnetic and thermal challenges in 5G arrays by integrating zooming and wide-angle scanning functionality into interleaved-shared layout aperiodic arrays with low side lobes. The effectiveness of the proposed method is demonstrated via simulations by using a 64-element array and its smartly thinned subsets.**

***Index Terms*—Antenna pattern synthesis, aperiodic array, beamwidth control, convex optimization, reconfigurable antenna.**

I. Introduction

THE introduction of the next-generation communication network, with the potential use of the millimeter-wave (mm-wave) frequencies for high-throughput, brings up many severe system challenges including, but not limited to, the increased product cost, implementation complexity, processing burden, and heat generation [1]. Although it is foreseen that digital beamforming solutions will prevail in the future due to their ability to provide the most flexible, accurate, and versatile performance, currently, the industrial baseline for beamforming in 5G antennas are mostly based on analog architectures that can generate a single beam at a time [2].

In such systems, it is necessary to (dynamically) determine the best (in terms of the signal-to-interference ratio) transmit and receive beam pairs between the base station and each user for a reliable multiuser communication [3]. If narrow and highly directive beams are used both at the transmit and receive sides, the system suffers from the large beam setup time and possible dramatic gain reduction due to slight beam misalignment [4]. Therefore, in the existing mm-wave standards (such as IEEE 802.15.3c [5] and IEEE 802.11ad [6]), multilevel beamforming procedures have been proposed. In these procedures, first, a transmitter and receiver find their best pairs using a wide (sectoral) beam, then, they narrow down their beamwidths gradually to a high-resolution pencil beam. The proposed adaptive beamwidth approach was also proven to be very efficient for the link setup in the current phase of the 5G systems [7]. Other works have proposed adaptive beamwidth control for effective user tracking in high-mobility scenarios [8] and for throughput improvement via increased spatial multiplexing or better diversity in multiple-input–multiple-output systems [9].

It is worth mentioning here that according to the beamwidth (and depending on the cell size), it might be necessary to adjust the input power to satisfy the demanding 5G mm-wave link budget requirements. Additionally, in 5G, it is desired, for each beam with a different resolution, to have a wide-angle scanning capability with low sidelobe levels (SLLs) in order to ensure a high quality-of-service (QoS) in the statistical sense [1].

A similar problem arises in satellite communication applications where multiple steerable (but in a very limited field-of-view when compared to 5G) and possibly reconfigurable (i.e., capable of switching between a set of beam shapes, creating zoomable beams, etc.) array antennas are aimed for high data rate flexible multispot coverage, together with low-rate broadcasting [10], [11]. Therefore, many pattern reconfigurable array synthesis techniques have been proposed in the literature and exploited particularly in arrays for satellite communications. These techniques include adaptively thinned [12]–[14] and interleaved/interleaved-shared arrays [15], together with phase-only (with/without amplitude tapering) [10], [16]–[18], position-phase [19], position-amplitude [11], amplitude-phase [20], or position-amplitude-phase [21] control.

Despite the variety of the design methods, currently proposed satellite antenna solutions have drawbacks in terms of the system cost, complexity (regarding the number of active antenna elements, beamforming architectures, signal processing, cooling, etc.) and they cannot handle the 5G's wider field-of-view as well as its thermal problem without a deeper theoretical revisit of different array topologies [22]. Among the existing array synthesis techniques listed as follows.

1) Adaptively thinned arrays were shown to be effective in thermal management [23], [24]. However, due to placing the elements on a fixed grid, the SLL suppression capability of thinned arrays for wide-angle scanning is very limited, especially for small and moderate array size [12].
2) Interleaved/interleaved-shared arrays efficiently use the available aperture to fit multiple arrays providing different resolution beams. Yet, the existing synthesis techniques of such arrays are only based on circularly symmetrical concentric rings, because of its appealing

Manuscript received May 3, 2020; revised June 15, 2020; accepted June 29, 2020. Date of publication July 1, 2020; date of current version September 3, 2020. This work was supported in part by the Netherlands Organisation for Scientific Research (NWO) and in part by NXP Semiconductors in the framework of the partnership program on Advanced 5G Solutions within the project 15590 titled "Antenna Topologies and Front-end Configurations for Multiple Beam Generation." *(Corresponding author: Yanki Aslan.)*

The authors are with the Department of Microelectronics, Microwave Sensing, Signals and Systems Group, Delft University of Technology, Delft 2600, The Netherlands (e-mail: y.aslan@tudelft.nl; a.g.roederer@tudelft.nl; a.yarovoy@tudelft.nl).

Digital Object Identifier 10.1109/LAWP.2020.3006314

geometry for easy optimization [15]. However, this topology supports only a limited number of different radial coordinates, which restricts its applicability for density tapering [25].

3) Amplitude and/or phase tapered arrays can achieve sufficient SLL suppression, but this comes at the expense of a significantly reduced array efficiency [26]. Moreover, since all the elements are active while generating both the narrow and wide beams, the heat generation in such arrays are much higher as compared to the thinned arrays.

In this letter, we introduce an array layout optimization technique that minimizes the maximal SLL within a predefined cell, for multiple steerable beams having distinct beamwidths. The technique uses the interleaved-shared layout approach introduced in [15] (but with full-flexibility in the element locations) and is based on an extension of the iterative convex position perturbation algorithm given in [27]. The key difference to [27] is the study of joint optimization schemes with different subset choices within a full array. The major advantages of the proposed approach are listed as follows.

1) The cooling challenge in the integrated 5G antennas is relaxed via power-efficient uniform-amplitude excitations and array subset activations (i.e., thinning) corresponding to the desired beam resolution.
2) By applying a smart irregularity in the array subset layouts, the SLLs are significantly reduced jointly for multiple wide-angle scanning varying-resolution beams.
3) Since the smaller-sized arrays generating wider beamwidths share their elements with the larger arrays, the total array aperture is efficiently used.

The combination of all these assets in an easy-to-solve and efficient optimization strategy creates the novelty of this work. The rest of this letter is organized as follows. Section II presents the problem formulation. The simulation results are discussed in Section III. The conclusions are given in Section IV.

II. Problem Formulation

To synthesize the array subset topologies for wide-angle scanning zoomable beams, the iterative convex position perturbation strategy in [27] is extended to optimization for multiple beamwidths. We start from a predefined array layout and move the nth element by ϵ_n^i in the x and δ_n^i in the $\hat{\mathrm{y}}$ direction at the ith step of the algorithm, which is represented as

$$x_n^i = x_n^{i-1} + \epsilon_n^i, \quad y_n^i = y_n^{i-1} + \delta_n^i. \tag{1}$$

The far-field expression can be linearized around the element locations using the first-order Taylor expansion when the following relation holds:

$$|k(u,v)(\epsilon,\delta)_n^i| \ll 1, \text{i.e., } |(\epsilon,\delta)_n^i| \ll \lambda/2\pi = 0.16\lambda \tag{2}$$

where $u = \sin\theta\cos\phi$ and $v = \sin\theta\sin\phi$. If the mutual coupling is ignored for simplicity, the far field expression of a scanned beam m $(m = 1, \ldots, M)$ using the array subset p $(p = 1, \ldots, P)$ at the ith iteration can be approximated as [27]

$$f_{\epsilon^i,\delta^i}^{i,m,p}(u,v) \approx \frac{E(u,v)}{(N_{p,f} - N_{p,l} + 1)} \sum_{n=N_{p,f}}^{N_{p,l}} e^{jk((u-u_m)x_n^{i-1})} e^{jk((v-v_m)y_n^{i-1})}(1 + jk(u-u_m)\epsilon_n^i + jk(v-v_m)\delta_n^i) \tag{3}$$

where $E(u,v)$ refers to the isolated (or the embedded, in large arrays) element pattern, the parameter set (u_m, v_m) denotes the steering position for the scanned beam m, while $N_{p,f}$ $(N_{p,l})$ labels the first (last) element in the array subset p. The vectors of parameters in the algorithm are defined as

$$\boldsymbol{\epsilon}^i = [\epsilon_{N_{p,f}}^i \cdots \epsilon_{N_{p,l}}^i]^T, \boldsymbol{\delta}^i = [\delta_{N_{p,f}}^i \cdots \delta_{N_{p,l}}^i]^T,$$
$$(\boldsymbol{U},\boldsymbol{V})_{SL}^p = [(\boldsymbol{u},\boldsymbol{v})_{SL,1}^p \cdots (\boldsymbol{u},\boldsymbol{v})_{SL,M}^p] \tag{4}$$

In (4), $\boldsymbol{\epsilon}^i$ and $\boldsymbol{\delta}^i$ include the position shifts in the x and $\hat{\mathrm{y}}$ directions, respectively, at the ith iteration. $(\mathbf{U},\mathbf{V})_{\mathrm{SL}}^p$ is a vector containing the (u,v) values forming the side lobe region for each scanned beam $m = 1, \ldots, M$ for the subset p. These regions are determined according to the angular definition of the sector $([-u_{\max}\ u_{\max}], [-v_{\max}\ v_{\max}])$, and a prespecified main beam radius of the array subset p, r_p, such that

$$(u,v) \in (\boldsymbol{u},\boldsymbol{v})_{\mathrm{SL},m}^p \text{ if } (u-u_m)^2 + (v-v_m)^2 > r_p^2 \text{ and } |u| \le u_{\max} \text{ and } |v| \le v_{\max}. \tag{5}$$

Furthermore, to guarantee a predefined minimum interelement spacing $d_{\min}$ in the final layouts, the distance between each element pair (α,β) is forced to be larger than $d_{\min}$ at each iteration using the following relation [27]:

$$(\epsilon_\alpha^i - \epsilon_\beta^i)(2x_\alpha^{i-1} - 2x_\beta^{i-1}) + (\delta_\alpha^i - \delta_\beta^i)(2y_\alpha^{i-1} - 2y_\beta^{i-1}) + (x_\alpha^{i-1} - x_\beta^{i-1})^2 + (y_\alpha^{i-1} - y_\beta^{i-1})^2 \ge d_{\min}^2. \tag{6}$$

Overall, the convex problem to be solved at the ith iteration of the algorithm is formulated as follows

$$\min_{\epsilon^i,\delta^i} \rho, \text{ s.t. } \begin{cases} \max|f_{\boldsymbol{\epsilon}^i,\boldsymbol{\delta}^i}^{i,p}((\mathbf{U},\mathbf{V})_{\mathrm{SL}}^p)| \le \rho \text{ for } \forall p \\ |\epsilon^i| \le \mu, \quad |\delta^i| \le \mu \\ (6) \text{ holds for } \forall(\alpha,\beta) \end{cases} \tag{7}$$

where ρ is the maximum SLL, which is simultaneously minimized for all the defined scanned beams $(m = 1, \ldots, M)$ and for all the allocated array subsets $(p = 1, \ldots, P)$. The position shifts $|\boldsymbol{\epsilon}^i|$ and $|\boldsymbol{\delta}^i|$ are upper bounded by a user-defined constant μ, which is limited to the value found in (2). The last constraint ensures that the minimum interelement distance at each iteration is larger than or equal to the a desired value, $d_{\min}$. The problem in (7) can be easily solved using freely available convex programming tools, such as CVX [28].

III. Simulation Settings and Results

The algorithm performance is shown considering $P = 3$ subsets of a 64-element array with a minimum interelement distance $(d_{\min})$ of 0.5λ. A 0.5λ-spaced square grid array is used at the input with initial subsets consisting of 64, 36, and 24 elements as shown in Fig. 1. Due to the convex nature of the proposed method, the selection (or labeling) of subsets is manually given. In other words, the algorithm does not automatically select the

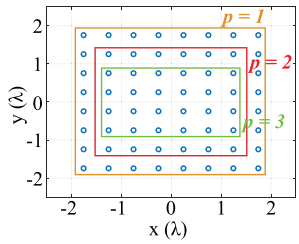

Fig. 1. Initial element locations and the three array subsets.

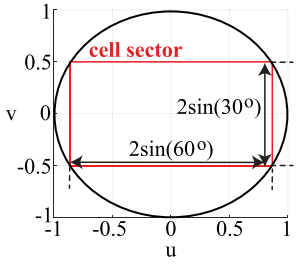

Fig. 2. Angular sector definition.

TABLE I
PERFORMANCE OF THE INITIAL ARRAY SUBSETS

Initial array topology	Max. SLL	Broadside directivity	Corner beam directivity
$p = 1$	-12.8 dB	23.0 dBi	20.4 dBi
$p = 2$	-12.4 dB	20.5 dBi	18.4 dBi
$p = 3$	-11.4 dB	18.8 dBi	17.0 dBi

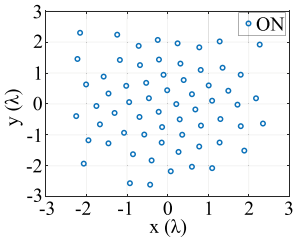

Fig. 3. Element locations optimized only for $p = 1$.

best elements needed for each subset, which can be seen as a limitation of the proposed approach.

A common embedded element pattern, $E(\theta, \phi) = \sqrt{\cos(\theta)}$ is assumed as a reasonable estimate for the average embedded pattern of identical elements with a minimum spacing and therefore, a maximum diameter of 0.5λ. In practice, the embedded element patterns (EEPs) are difficult to compute in such an irregular array. They would depend on the type of the elements used and on their position in the array. Also, in the case of linearly polarized elements SLL might somewhat differ in the E- and H-planes. Note that it is possible to include the effect of mutual coupling in the proposed optimization routine (for any type of radiator element) by performing EEP simulations at each iteration, as done in [29] and [30], which is not considered in this article due to the computational complexity.

The sector is defined by ±60°/±30° in azimuth/elevation (see Fig. 2). The varying-resolution beams are jointly optimized for the broadside and eight scan positions along the sector edges and corners ($M = 9$). The parameter r_p is equal to 0.25, 0.33, and 0.4 for the 64-, 36-, and 24-element subsets, respectively. The u-v plane is discretized in steps of 0.01. The upper bound for the position shifts $\mu = 0.04\lambda$ is used for stable convergence. Table I shows the SLLs and directivities of the initial subsets, which are given as benchmarks for performance comparison with the optimized subsets.

A. *Optimization for a Single Subset:* $p = 1/p = 2$ *or* $p = 3$

First, we consider a single subset optimization. Figs. 3 and 4 show the element locations and the SLL trend when the topology is optimized only for $p = 1$. It is seen that maximum SLL in the sector (w.r.t. the broadside gain) becomes as low as −22.6 dB, which is kept also for the scanned beams (see Fig. 5). It is also seen that the broadside directivity slightly

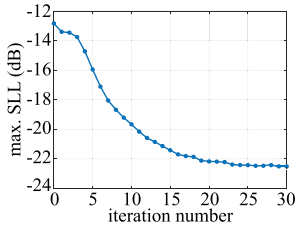

Fig. 4. SLL trend (w.r.t. broadside gain), optimized for $p = 1$.

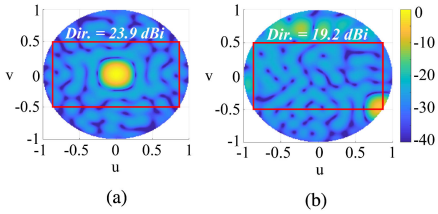

Fig. 5. Radiation pattern (normalized w.r.t. broadside gain, in dB) of the 64-element array optimized for $p = 1$. (a) Broadside beam. (b) Corner beam.

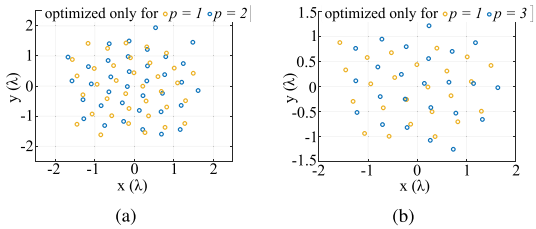

Fig. 6. Layout comparisons for single subset optimization. (a) 36 elements. (b) 24 elements.

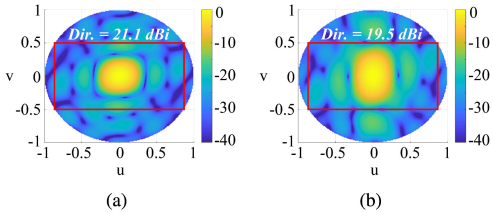

Fig. 7. Broadside radiation pattern (normalized, in decibel) using subsets of the array optimized only for $p = 1$. (a) 36 elements. (b) 24 elements.

increases (∼1–1.5 dB), while the corner beam directivity slightly decreases (∼1–1.5 dB) as compared to the reference values given in Table I. This observation is valid for all the optimized subsets given throughout this letter.

When the subsets $p = 2, 3$ (as initially labeled in Fig. 1) are extracted from the optimized layout given in Fig. 3 (see Fig. 6), the first SLL can reach up to −15.3 dB, which is visualized in Fig. 7. On the other hand, if the optimization is solely performed on the 36- and 24-element arrays, different optimal layouts are obtained (as in Fig. 6) that are able to reduce the SLL to −20.2 dB and −18.6 dB, respectively (see Fig. 8). This analysis clearly highlights the motivation to seek for a "better" topology jointly optimized for several subsets.

B. *Optimization for Two Subsets:* $p = 1, 2$

In this part, the 64-element layout is simultaneously optimized for $p = 1$ and $p = 2$. The resulting element locations are given in Fig. 9. From Fig. 10(a), it can be seen that using the subsets of the jointly optimized layout, the maximum SLL is reduced to

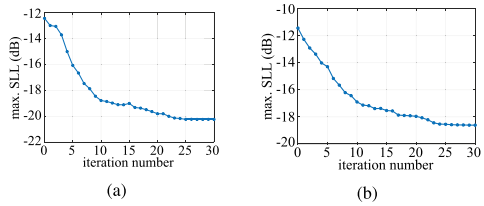

Fig. 8. SLL trend (w.r.t. broadside gain) with subset layout optimization for: (a) 36 elements: $p = 2$ and (b) 24 elements: $p = 3$.

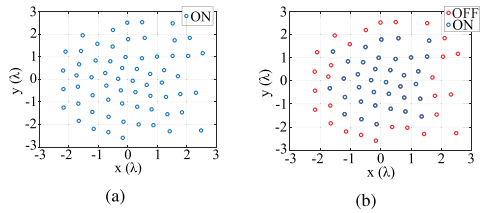

Fig. 9. Element locations optimized for $p = 1, 2$. (a) 64 elements: $p = 1$. (b) 36 elements: $p = 2$.

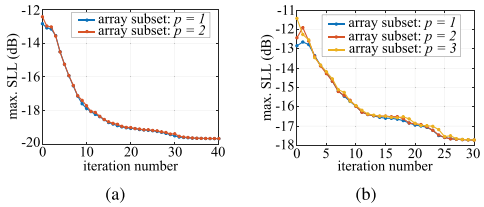

Fig. 10. SLL trend (w.r.t. broadside gain) of the array subsets with joint layout optimization for: (a) $p = 1, 2$, (b) $p = 1, 2$, and 3.

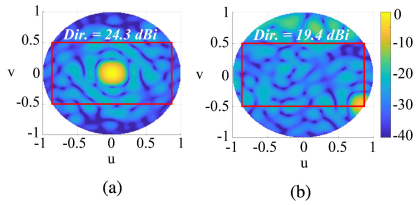

Fig. 11. Radiation pattern (normalized w.r.t. broadside gain, in dB) of the 64-element array optimized for $p = 1, 2$. (a) Broadside. (b) Corner beam.

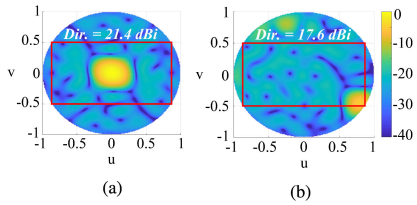

Fig. 12. Radiation pattern (normalized w.r.t. broadside gain, in dB) of the 36-element subset optimized for $p = 1, 2$. (a) Broadside. (b) corner beam.

-19.7 dB for both the 64- and 36-element arrays. The achieved SLL is maintained when the beam is scanned inside the sector, as visualized in Figs. 11 and 12.

C. *Optimization for Three Subsets:* $p = 1, 2, 3$

Finally, we optimize the layout jointly for the three array subsets, which results in the element locations provided in Fig. 13. The SLL trend given in Fig. 10(b) shows a maximum SLL of -17.7 dB, which is common for all the three subsets.

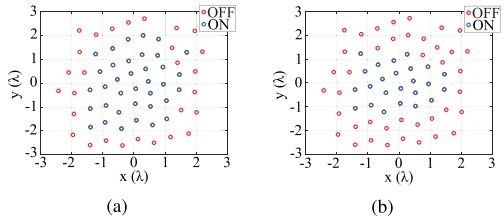

Fig. 13. Element locations optimized for $p = 1, 2, 3$. (a) 36 elements: $p = 2$. (b) 24 elements: $p = 3$. (Note that all elements are ON for $p = 1$).

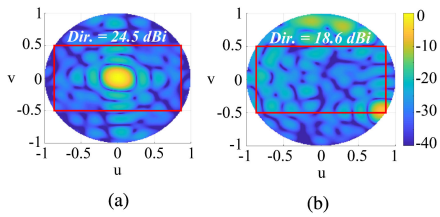

Fig. 14. Radiation pattern (normalized w.r.t. broadside gain, in dB) of the 64-element array optimized for $p = 1, 2$, and 3. (a) Broadside. (b) Corner beam.

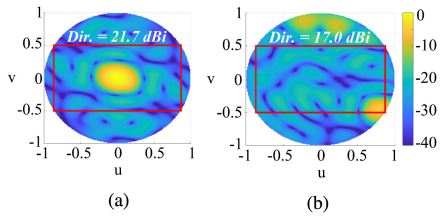

Fig. 15. Radiation pattern (normalized w.r.t. broadside gain, in dB) of the 36-element subset optimized for $p = 1, 2$, and 3. (a) Broadside. (b) Corner beam.

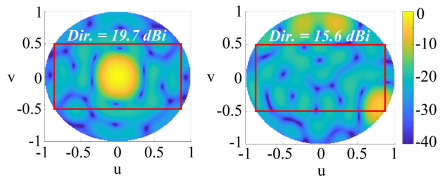

Fig. 16. Radiation pattern (normalized w.r.t. broadside gain, in dB) of the 24-element subset optimized for $p = 1, 2$, and 3. (a) Broadside. (b) Corner beam.

For completeness, the scanning performance of the arrays for the layout in Fig. 13 are visualized in Figs. 14–16 for the 64-, 36-, and 24-element subsets, respectively.

IV. Conclusion

An optimal array (subset) layout synthesis technique has been proposed that minimizes the maximal SLL for multiple steerable beams having distinct beamwidths (zoom-in/-out functionality), which is to be used for efficient link setup and high QoS communication in 5G. The simulation results have shown that joint layout optimization for multiple uniformly fed array subsets provides an advantageous suboptimal balance among the SLL suppression capabilities of different array portions. The achieved SLL is maintained at all the subsets, even for wide-angular scanning. Further SLL suppression or null formation can be achieved using amplitude/phase tapering, at the expense of reduced power efficiency.

REFERENCES

[1] Y. Aslan, J. Puskely, A. Roederer, and A. Yarovoy, "Trade-offs between the quality of service, computational cost and cooling complexity in interference-dominated multi-user SDMA systems," *IET Commun.*, vol. 14, no. 1, pp. 144–151, Jan. 2020.

[2] Y. Aslan, C. E. Kiper, A. J. van den Biggelaar, U. Johannsen, and A. Yarovoy, "Passive cooling of mm-wave active integrated 5G base station antennas using CPU heatsinks," in *Proc. 16th Eur. Radar Conf.*, Paris, France, Oct. 2019, pp. 121–124.

[3] F. Fuschini, M. Zoli, E. M. Vitucci, M. Barbiroli, and V. Degli-Esposti, "A study on millimeter-wave multiuser directional beamforming based on measurements and ray tracing simulations," *IEEE Trans. Antennas Propag.*, vol. 67, no. 4, pp. 2633–2644, Apr. 2019.

[4] K. C. Joshi, S. Niknam, R. V. Prasad, and B. Natarajan, "Analyzing the tradeoffs in using millimeter wave directional links for high data-rate tactile internet applications," *IEEE Trans. Ind. Informat.*, vol. 16, no. 3, pp. 1924–1932, Mar. 2020.

[5] *IEEE Standard for Information Technology—Local and Metropolitan Area Networks—Specific Requirements—Part 15.3: Amendment 2: Millimeter-Wave-Based Alternative Physical Layer Extension*, IEEE Standard 802.15.3c-2009, 2009.

[6] I. C. S. L. S. Committee *et al.*, *IEEE Standard for Information Technology-Telecommunications and Information Exchange Between Systems-Local and Metropolitan Area Networks-Specific Requirements Part 11: Wireless LAN Medium Access Control (MAC) and Physical Layer (PHY) Specifications*, IEEE Standard 802.11, 2007.

[7] K. Chandra, R. V. Prasad, I. G. M. M. Niemegeers, and A. R. Biswas, "Adaptive beamwidth selection for contention based access periods in millimeter wave WLANs," in *Proc. IEEE Consum. Commun. Netw. Conf.*, Las Vegas, NV, USA, Jan. 2014, pp. 458–464.

[8] H. Chung and S. Kim, "Adaptive beamwidth control for mmWave beam tracking," Jul. 2019, [Online]. Available: arXiv:1907.08753

[9] V. Sergeev, A. Davydov, G. Morozov, O. Orhan, and W. Lee, "Enhanced precoding design with adaptive beam width for 5G new radio systems," in *Proc. IEEE 86th Veh. Technol. Conf.*, Toronto, ON, Canada, Sep. 2017, pp. 1–5.

[10] O. M. Bucci, S. Perna, and D. Pinchera, "Synthesis of isophoric sparse arrays allowing zoomable beams and arbitrary coverage in satellite communications," *IEEE Trans. Antennas Propag.*, vol. 63, no. 4, pp. 1445–1457, Apr. 2015.

[11] C. Bencivenni, M. V. Ivashina, and R. Maaskant, "Reconfigurable aperiodic array synthesis by compressive sensing," in *Proc. 10th Eur. Conf. Antennas Propag.*, Davos, Switzerland, Apr. 2016, pp. 1–3.

[12] R. L. Haupt, "Adaptively thinned arrays," *IEEE Trans. Antennas Propag.*, vol. 63, no. 4, pp. 1626–1632, Apr. 2015.

[13] R. Jain and G. S. Mani, "Dynamic thinning of antenna array using genetic algorithm," *Prog. Electromagn. Res. B*, vol. 32, pp. 1–20, 2011.

[14] Y. Liu, P. You, C. Zhu, X. Tan, and Q. H. Liu, "Synthesis of sparse or thinned linear and planar arrays generating reconfigurable multiple real patterns by iterative linear programming," *Prog. Electromagn. Res.*, vol. 155, pp. 27–38, 2016.

[15] O. M. Bucci, S. Perna, and D. Pinchera, "Interleaved isophoric sparse arrays for the radiation of steerable and switchable beams in satellite communications," *IEEE Trans. Antennas Propag.*, vol. 65, no. 3, pp. 1163–1173, Mar. 2017.

[16] A. F. Morabito, A. Massa, P. Rocca, and T. Isernia, "An effective approach to the synthesis of phase-only reconfigurable linear arrays," *IEEE Trans. Antennas Propag.*, vol. 60, no. 8, pp. 3622–3631, Aug. 2012.

[17] Y. Liu, Y.-C. Jiao, Y.-M. Zhang, and Y.-Y. Tan, "Synthesis of phase-only reconfigurable linear arrays using multiobjective invasive weed optimization based on decomposition," *Int. J. Antennas Propag.*, vol. 2014, pp. 1–11, Oct. 2014.

[18] G. Buttazzoni and R. Vescovo, "Reconfigurable array synthesis with constraints on near field, far field and dynamic range ratio," in *Proc. IEEE Int. Conf. Electromagn. Adv. Appl.*, Turin, Italy, Sep. 2009, pp. 257–260.

[19] D. Jamunaa, G. Mahanti, and F. N. Hasoon, "Synthesis of phase-only position optimized reconfigurable uniformly excited linear antenna arrays with a single null placement," *J. King Saud Univ. Eng. Sci.*, Apr. 2019, to be published.

[20] D. Gies and Y. Rahmat-Samii, "Particle swarm optimization for reconfigurable phase-differentiated array design," *Microw. Opt. Technol. Lett.*, vol. 38, no. 3, pp. 172–175, Aug. 2003.

[21] Y. Liu, Q. H. Liu, and Z. Nie, "Reducing the number of elements in multiple-pattern linear arrays by the extended matrix pencil methods," *IEEE Trans. Antennas Propag.*, vol. 62, no. 2, pp. 652–660, Feb. 2014.

[22] Y. Aslan, J. Puskely, A. Roederer, and A. Yarovoy, "Active multiport subarrays for 5G communications," in *Proc. IEEE Top. Conf. Antennas Propag. Wireless Commun.*, Granada, Spain, Sep. 2019, pp. 298–303.

[23] D. B. Peterson, "Adaptive thinning of an active electronic scan antenna for thermal management," Eur. Patent EP3 467 937A1, Feb. 10, 2018.

[24] Y. Aslan, J. Puskely, J. H. J. Janssen, M. Geurts, A. Roederer, and A. Yarovoy, "Thermal-aware synthesis of 5G base station antenna arrays: an overview and a sparsity-based approach," *IEEE Access*, vol. 6, pp. 58868–58882, 2018.

[25] M. C. Vigano, G. Toso, G. Caille, C. Mangenot, and I. E. Lager, "Sunflower array antenna with adjustable density taper," *Int. J. Antennas Propag.*, vol. 2009, Jan. 2009, Art. no. 624035.

[26] Y. Aslan, J. Puskely, A. Roederer, and A. Yarovoy, "Phase-only control of peak sidelobe level and pattern nulls using iterative phase perturbations," *IEEE Antennas Wireless Propag. Lett.*, vol. 18, no. 10, pp. 2081–2085, Oct. 2019.

[27] Y. Aslan, J. Puskely, A. Roederer, and A. Yarovoy, "Multiple beam synthesis of passively cooled 5G planar arrays using convex optimization," *IEEE Trans. Antennas Propag.*, vol. 68, no. 5, pp. 3557–3566, May 2020.

[28] M. Grant and S. Boyd, "CVX: Matlab software for disciplined convex programming, version 2.1," Mar. 2014. [Online]. Available: http://cvxr.com/cvx

[29] Y. Aslan, M. Candotti, and A. Yarovoy, "Synthesis of multi-beam space-tapered linear arrays with side lobe level minimization in the presence of mutual coupling," in *Proc. 13th Eur. Conf. Antennas Propag.*, Krakow, Poland, Apr. 2019, pp. 1–5.

[30] H. B. Van, S. N. Jha, and C. Craeye, "Fast full-wave synthesis of printed antenna arrays including mutual coupling," *IEEE Trans. Antennas Propag.*, vol. 64, no. 12, pp. 5163–5171, Dec. 2016.